PHOTON-COUNTING MICROLASER RANGERS, TRANSPONDERS, AND ALTIMETERS

John J. Degnan
Geoscience Technology Office, Code 920.3
NASA Goddard Space Flight Center
Greenbelt, MD 20771 USA

ABSTRACT

Unlike current manned systems, NASA's next generation SLR2000 Satellite Laser Ranging (SLR) station is fully autonomous, eye-safe, relatively compact and inexpensive, and, during daytime tracking, operates at signal-to-noise ratios several orders of magnitude below unity. Tiny, passively Q-switched microlasers generate ultra-short pulses with output energies on the order of 100 μJ at few kHz rates to achieve mm-level ranging precision to satellite altitudes of 20,000 km. Special ranging receivers, combined with Poisson statistical analysis of the received photon distribution, enable the system to rapidly and reliably identify and extract the single photon laser echoes from the solar background. The enhanced rate of return, combined with a uniform signal strength, can actually drive down both systematic and random range errors. The new SLR2000 technology has already spawned exciting new applications. Compact microlaser altimeters, capable of mapping the surface of a planet or other celestial body at multikilohertz rates, is one such application, and a high altitude, airborne version is currently being developed under NASA's Instrument Incubator Program. Interplanetary microlaser transponders would be capable of performing decimeter ranging or subnanosecond time transfer to spacecraft throughout the inner Solar System, resulting in improved knowledge of planetary motions and librations and enhanced General Relativity experiments.

1. INTRODUCTION

The Geoscience Technology Office within the Laboratory for Terrestrial Physics at NASA's Goddard Space Flight Center is currently investigating several new photon counting laser instruments to meet the needs of a variety of science applications. These include the automated SLR2000 Satellite Laser Ranging (SLR) station, a Breadboard Interplanetary Laser Transponder, and a Multikilohertz Microlaser Altimeter ("Microaltimeter"), each of which is discussed in subsequent sections. The aforementioned instruments have some common features, i.e. they all are characterized by:

- Multi-kilohertz laser fire and sampling rates (2 to 10 kHz)
- Single photon detection at 532 nm
- A 24 hour operational capability
- Mean signal strengths less than one photoelectron per laser fire
- Signal-to-Noise Ratios (SNR) much less than unity during daylight operations
- Subnanosecond pulsewidths for high ranging precision
- Small to modest telescope apertures (14 to 40 cm)
- Moderate to low laser output powers on the order of a watt or less generated by a compact, passively Q-switched microlaser measuring a few cms in length.

2. LIDAR EFFICIENCY AS MOTIVATION FOR SINGLE PHOTON DETECTION

Regardless of whether one is discussing rangers, altimeters or transponders, the mean number of signal photoelectrons recorded by the receiver on a single laser fire is given by a lidar link equation of the form

$$n_s = \frac{C_X E_t A_r}{R^{N_X}} \tag{1}$$

where E_t is the transmitter energy, A_r is the area of the receiving telescope, R is the one-way distance between the source and the target, C_X is a constant for each type of system, and the subscript X is replaced by R for Ranger, A for Altimeter, and T for Transponder. For altimeters and transponders, $N_X = N_T = 2$

whereas for rangers $N_R = 4$. Also, for rangers and altimeters, the transmitted energy and receive aperture in (1) are collocated at the same terminal whereas, for transponders, the transmitted energy and receive aperture in (1) refer to the values at opposite terminals. For each type of system, the multiplicative constants C_X are given by

$$C_R = \frac{4\eta_q \eta_t \sigma_t \eta_r T_a^2}{h\nu\theta_t^2 (4\pi)^2} \tag{2a}$$

$$C_A = \frac{\eta_q \eta_t \rho \eta_r \cos\sigma_s T_a^2}{\pi h\nu} \tag{2b}$$

$$C_T = \frac{4\eta_q' \eta_t \eta_r' T_a T_a'}{h\nu\theta_t^2 (4\pi)} \tag{2c}$$

for rangers, altimeters, and transponders respectively. Parameters common to all systems are the detector quantum efficiency η_q, the photon energy hv, the one-way atmospheric transmission T_a, the divergence half-angle of the laser beam θ_t, and the optical throughput efficiencies of the transmitter (η_t) and receiver (η_r) optics respectively. In the transponder constant, primed and unprimed values correspond to the parameters at the receiving and transmitting terminals respectively. The altimeter constant contains two unique parameters, i.e. the surface reflectance, ρ, and the surface slope, σ_s. We can choose to write (1) in terms of the average laser power, i.e.

$$n_s = \frac{C_X P_t A_r}{f_{QS} R^{N_X}} \tag{3}$$

where f_{QS} is the Q-switching frequency (laser fire rate) in Hz.

One measure of a lidar's operating efficiency is the number of measurements that can be obtained with a given power-aperture product, P_tA_r. The number of samples or measurements per second is given by the product of the fire rate and the probability of detection , i.e.

$$f_S = f_{QS} P_D(n_s, n_t) = f_S^{\max}\left[\frac{1}{n_s}\left(1 - e^{-n_s}\sum_{k=0}^{n_t-1}\frac{n_s^k}{k!}\right)\right] \tag{4}$$

where the probability of detection in the low signal limit is given by Poisson statistics and depends on both the mean signal strength, n_s, and the detection threshold, n_t,. In deriving (4), we have solved (3) for f_{QS} and defined a maximum sampling rate

$$f_S^{\max} = \frac{C_X P_t A_r}{R^{N_X}} \tag{5}$$

In Figure 1, we plot the normalized return rate, f_s/f_s^{max}, and demonstrate that the parameter f_s^{max} does indeed correspond to the maximum sampling rate in the limit of small mean signal strength. We make the following observations:

For a given laser power and receive aperture, the maximum sampling rate (lidar efficiency) is obtained by using single photon detection and a high repetition rate laser with low energy per pulse such that the mean signal count per laser fire is $n_s << 1$.

For higher thresholds, the sampling frequency peaks, at a value lower than f_s^{max}, for mean signal counts near the threshold value (e.g. at n_s = 1.8 pe for n_t = 2 pe and at n_s = 3.3 pe for n_t = 3 pe, etc.).

To achieve comparable sampling rates at thresholds higher than one photoelectron, the instrument power-aperture product would have to be increased significantly (e.g. by factors of 3.4 and 5.1 for thresholds of 2 and 3 pe respectively). Conventional spaceborne laser altimeters constructed to date operate in the infrared (1064 nm) at thresholds on the order of 100 pe so their "lidar efficiency" is greatly reduced.

3. EXTRACTING THE SIGNAL FROM THE NOISE BACKGROUND

The results of Section 2 are interesting, but real photon counting systems designed to operate in daylight must contend with a rather heavy noise background. For an Earth-based satellite laser ranging station, scattered sunlight from the atmosphere within the receiver field of view (FOV) is the primary source of background noise. For a transponder on the surface of Mars, the situation is similar except the noise levels are significantly lower due to the reduced solar flux at Mars and a much thinner atmosphere which has fewer scattering particles. In an altimeter, on the other hand, the solar background is produced by radiation scattered from both the interrogated surface and the intervening atmosphere. Photodetector "dark counts" are another CW source of noise, but the dark count rate tends to be relatively low relative to the solar background (especially in visible detectors) and can often be ignored. Backscattered laser radiation can also contribute significantly to the noise background for short time intervals immediately following the laser fire. The instrument sensitivity to locally backscattered laser radiation is largely dependent on whether or not (1) the detector is gated or (2) the instrument is bistatic (i.e. has separate transmit/receive optics as opposed to common optics) and/or is located within an atmosphere. Thus, compared to a lander, transponders in spacecraft cruise phase or in orbit about another planet have a vastly more benign noise environment since the noise background originates from the distant Earth and other celestial objects (e.g. the Moon and stars) within the transponder FOV. However, strict control of stray light emanating from outside the instrument FOV is essential, especially if one is looking very close to the Sun.

Thus, the first step in designing a viable photon counting lidar is to reduce the noise background as much as possible. This can be accomplished through the use of various types of filters. Specifically, one can limit the width of the bandpass filter ("spectral filtering"), reduce the field-of-view of the receiver to the minimum value which encompasses the transmit beam divergence and its potential pointing variations and/or coalignment errors with the receiver ("spatial filtering"), and gate the receiver so that only photons within a given time window about the expected signal return are accepted ("temporal filtering").

In high energy multi-photon systems, one has the additional option of raising the detection threshold until there is an acceptably low number of noise-induced false alarms ("amplitude filtering"). In the photon counting world, however, one must accept a large number of detected noise counts during daylight pperations and use statistical expectations over multiple laser fires to discriminate between signal and noise ("Post-Detection Poisson Filtering" or PDPF). Such a statistical filter was successfully used in the early 1970's to identify single photons reflected from passive reflectors placed on the Moon in early Lunar Laser Ranging (LLR) experiments [Abbott and Shelus, 1973]. A PDPF is crucial to photon-counting systems where the mean number of noise photoelectrons generated within the range gate per laser fire often greatly exceeds the mean number of signal photoelectrons, which is usually less than one.

PDPF's are similar in concept to "lock-in amplifiers", which take advantage of the fact that the signals occurring at a fixed frequency are bunched together in time, or "temporally coherent", whereas the dominant background noise is randomly distributed in time, or "temporally incoherent". For example, if a range window or "gate" (representing the range uncertainty) is separated into properly sized time bins and displayed as a histogram, repeated measurements of the round trip times-of-flight (TOF's) to a fixed target will fall into a single bin with the noise counts randomly distributed amongst all the bins to yield a noise

floor. The more frequent and accurate the range measurements relative to the noise count per bin, the more rapidly the signal bin population will rise above the noise floor within the overall TOF histogram.

In the three applications to be discussed here (ranger, transponder, and altimeter), the range between instrument and target is changing rapidly, and hence the expected signal will not be "temporally coherent" with respect to the laser fire time. However, if one applies appropriate corrections and/or constraints to the time-of-flight (TOF) measurements based on a priori knowledge of the range and range rate between the instrument and target, the range-corrected signal distribution will be significantly more highly peaked in range space than the raw range data and can be viewed as "quasi-coherent" for some finite length of time.

3. SLR2000 AUTONOMOUS SATELLITE LASER RANGING STATION

Unlike current manned Satellite Laser Ranging (SLR) systems, NASA's next generation SLR2000 system, shown in Figure 2, is designed to be fully autonomous and eye-safe and to perform millimeter precision ranging to the full constellation of retroreflector-equipped satellites at altitudes up to 20,000 km above sea level [Degnan and McGarry, 1997; Degnan, 1998]. Like its manned predecessors, SLR2000 has numerous scientific applications including maintenance of the terrestrial reference frame, precise orbit determination, geophysics, gravity, fundamental physics, and global time transfer. Although 532 nm is in the visible and not an "eye-safe" wavelength, SLR2000 achieves eye safety by reducing the transmitted single pulse energy by almost three orders of magnitude (from 100 mJ for the manned NASA MOBLAS system to 135 μJ) and by utilizing the full aperture of the common transmit/receive telescope in transmitting the laser energy. The MOBLAS system also has a larger receive aperture (76 cm vs 40 cm), resulting in an overall single shot signal advantage for MOBLAS of almost 2667 to 1 relative to SLR2000.

To narrow this huge discrepancy in the number of received photons, the SLR2000 system is operated at a much higher 2 kHz rate compared to 5 Hz for MOBLAS. Thus, the time-averaged transmitted laser power for SLR2000 of 270 mW (135 μJ at 2 kHz) is within a factor of 2 of the 500 mW transmitted by the conventional high power MOBLAS station (100 mJ at 5 Hz). Furthermore, the exceptional quasi-TEM_{00} spatial mode quality of the microlaser transmitter permits the laser beam divergence to be narrowed from roughly 30 arcseconds to 10 arcseconds so that a significantly greater fraction of the energy is concentrated on the target. The resulting factor of 9 beam divergence advantage, multiplied by the factor of 400 repetition rate advantage, actually gives SLR2000 a slight edge (3600/2667 = 1.35) over MOBLAS with respect to the mean number of photons received per unit time.

During laser tracking, the range data is usually displayed for the operator on an "Observed Minus Calculated" or "O-C" plot. In this plot, the signal data is plotted relative to the center of the range gate, which is continually being adjusted based on fairly precise a priori knowledge of the relative motion between the station and satellite. Thus, if our relative motion model and gating implementation were perfect and there were no instrumental biases, the corresponding O-C plot would place all of the signal photons within a single narrow range bin centered in the range gate, in a manner totally indistinguishable from our previous fixed target example. Solar-induced noise photons and detector dark counts, on the other hand, would be randomly distributed throughout the gate. In this highly idealized case, the temporal width of the signal data distribution would then be determined by the timing precision of the range receiver and small atmosphere-induced fluctuations. In the most accurate SLR systems, the data is characterized by a one sigma RMS single-shot range scatter of about one cm [Degnan, 1993]. This corresponds to a scatter in the TOF of only 67 picoseconds, representing a very high state of temporal coherence. Within such a narrow single temporal bin on the order of 100 psec, a 1 MHz noise rate in the instrument would produce only one noise count for every 10,000 laser fires. In the same amount of time, even a very weak mean signal count on the order of 0.001 pe per laser fire produces 10 counts plus 1 noise count equals 11 counts in the signal bin (or a ***signal cell contrast*** of 11 to 1), making it easily distinguishable from the noise.

In real SLR systems, a range bias and imperfect knowledge of the relative motion between the instrument and target will respectively introduce a displacement of the signal data from the center of the range gate and a slope in the signal data as viewed in the O-C reference frame. This is illustrated in Figure 3, which shows a simulation of SLR2000 acquiring the LAGEOS satellite at 20 degrees elevation, corresponding to a one-way slant range of approximately 8300 km. During LAGEOS acquisition, the SLR2000 mean signal

count per laser fire is often below 0.001 photoelectrons (pe). Although the signal count rises rapidly with elevation angle due to both decreasing range and improved atmospheric transmission, it never exceeds 1 pe. In Figure 3, the signal counts selected by the auto-tracking algorithm (to be discussed later) are plotted as darker dots against a dense noise background of lighter dots. No signal appears during the early phases of the simulated acquisition because the simulator assumed an angular pointing error, which caused the beam to miss the target so that no signal photons were generated. The simulator then initiated an outwardly spiraling search sequence to find the target. When the beam finally falls on the target at roughly 85 seconds into the acquisition, the correctly identified "data" has a downward slope caused by a simulated time bias in the orbit prediction. Based on the observed slope, the auto-tracking algorithm estimates and applies the corresponding time bias to the range prediction data to iteratively reduce the slope and improve the "temporal coherence" of the O-C plot. This allows the range gate to be narrowed (note the tightening of the gray noise counts in the vertical) as well as the range bins, which in turn improves the signal cell contrast and reduces the "frame" time necessary to reliably differentiate between signal and noise. The algorithm also computes and applies a range bias in order to keep the signal centered within the gate.

Thus, even in the presence of a small time bias (range rate error), the signal data will still be highly confined in O-C space for appropriately short time intervals (called a "frame"). However, the residual range and range-rate uncertainties during target acquisition force us to initially widen the range bins, beyond the minimum required by the instrumental precision, in order to retain a high probability of capturing all of the signal photoelectrons received in the sequence of laser fires defining the frame. Once the signal is acquired, however, the residual uncertainties in both range and range rate can be iteratively reduced along with range gates, bin sizes, and frame times for virtually noise-free tracking.

4. INTERPLANETARY MICROLASER TRANSPONDERS

The ability to use "temporal coherence" to extract a weak satellite ranging signal as small as 0.0001 pe from the much stronger solar background led us to consider asynchronous interplanetary microlaser transponders [Degnan, 1996; Degnan et al, 1998]. Such transponders would permit decimeter accuracy or better ranging and subnanosecond time transfer between Earth and a spacecraft operating anywhere within the inner Solar System, e.g. out to the asteroid belt beyond Mars. Science applications would include precise planetary or asteroid ephemeredes and librations, solar system physics, and enhanced General Relativity experiments carried out on an interplanetary scale.

In an asynchronous transponder, the two terminals independently fire pulses at each other at a common laser fire rate, f_{QS}, as in Figure 4. Terminal A records the times of departure of its own transmitted pulses and the (possibly intermittent) times of arrival of pulses from "B" and vice versa. The departure and arrival times measured at each terminal are then communicated to, and properly paired at, a common processor which then calculates a range and clock offset for the two terminals via the equations [Degnan, 1996]

$$R = \frac{c}{2}\left(t_{EM} + t_{ME}\right) = \frac{c}{2}\left[\left(t_{E2} - t_{E1}\right) + \left(t_{M2} - t_{M1}\right)\right] \tag{6}$$

and

$$\tau = \frac{\left[\left(t_{E2} - t_{E1}\right) - \left(t_{M2} - t_{M1}\right)\right]}{2\left(1 + \frac{\dot{R}}{c}\right)} \tag{7}$$

where the intervals $\left(t_{E2} - t_{E1}\right)$ and $\left(t_{M2} - t_{M1}\right)$ are measured by the Earth and spacecraft range receivers respectively. In (6) and (7), R and τ are the instantaneous range and clock offset at the point in time when the "photon world lines" marked t_{EM} and t_{ME} in Figure 4 cross each other. In (7), the small correction term,

$\dot{R}/c$, corresponding to the instantaneous range rate between the Earth station and the spacecraft divided by the speed of light, can be estimated from planetary ephemeredes or the microwave communications link or iteratively solved for from the laser range data.

Severe size, weight, and prime power limitations on interplanetary spacecraft typically preclude both the use of large and powerful laser transmitters to enhance the signal strength at the Earth station as well as the use of large telescopes to increase the signal strength at the spacecraft. Fortunately, one can place as much of the transponder link burden on the Earth station as necessary (within practical or economic limits) to achieve a "balanced" link, i.e. one in which both terminals detect signals from the opposite terminal at roughly the same rate [Degnan et al, 1998]. This can be seen from the link equation (1) where, uniquely for the transponder case, E_t and A_r refer to the transmitted laser energy and receiver area at opposite terminals. Nevertheless, there is much to be gained from a size, weight, and power efficiency standpoint if one operates in single photon detection mode at both ends of the link. This is especially true when one considers interplanetary distances of several hundred million km and the R^{-2} dependence on signal strength. For this reason, we considered an Earth-Mars transponder link which used SLR2000, slightly modified to handle the larger transmitter point ahead angles, as the Earth station [Degnan, et al, 1998]. A breadboard transponder, sized for a Mars lander and shown in Figure 5, was built to simulate range and time transfer in laboratory experiments with the prototype SLR2000 receiver. The breadboard uses a 14.7 cm diameter shared-aperture telescope and an SLR2000 transmitter producing 135 μJ per pulse at 2 kHz. Simulations have demonstrated a capability of making thousands to tens of thousands of individual range measurements per minute over the full range of Earth-Mars distances, from 0.52 to 2.52 AU [Degnan, 1996].

Although not essential, the use of a common laser fire rate in the double-ended transponder link simplifies the instrument and forces a degree of temporal coherence between the departure of the pulse from Terminal A and the arrival of the pulse from Terminal B which is inherent in the single-ended ranger. Recalling our previous examples of a fixed target or an O-C plot with perfectly modeled relative motion between the two terminals, a correlation range receiver, which plots the received signal times modulo the laser fire interval (500 μsec for SLR2000), would rapidly produce a highly peaked histogram which clearly identified the signal bin. This would be true in spite of the fact that pulses leaving the two instruments at roughly the same time require many minutes (corresponding to millions of laser fire intervals) to reach the opposite terminal. However, for an asynchronous transponder, a residual slope in the O-C curve could result not only from imperfect knowledge of the relative motion between the two terminals but also a mean frequency offset between the Earth and spacecraft clocks. As in the SLR example, the autotracking algorithm estimates and applies the observed range-rate error to the range prediction data to iteratively reduce the observed slope, improve the "temporal coherence" of the O-C plot, narrow the range gate, enhance the signal cell contrast by reducing the range bin size, and reduce the "frame" time necessary to reliably differentiate between signal and noise. The algorithm also computes and applies an observed range bias to center the signal within the gate.

5. MULTIKILOHERTZ MICROLASER ALTIMETER

Under NASA's Instrument Incubator Program (IIP), we are currently building a photon counting airborne microlaser altimeter, or "microaltimeter", based on these concepts [Degnan, 2000]. The instrument is designed to operate at a 10 kHz rate from aircraft cruise altitudes in the range 7 to 12 km with a single pulse energy of less than 10 μJ and a single 14 cm diameter off-axis telescope, which is spatially shared by the transmitter and receiver. The system also uses multi-anode metal dynode chain photomultipliers in order to segment the ground image into as many as 16 pieces (4x4 "pixels"). Each of the anodes is input to an independent timing channel so that the altimeter can be operated in a 3D quasi-imaging mode. For increased portability between aircraft, the instrument is packaged to fit into a standard Lyca camera mount, which is widely used in airborne photogrammetry systems.

The use of photon counting receivers in altimetry introduces some additional complications which are not encountered in either the ranger or transponder. First of all, the return pulse is broadened by the surface slope and roughness within the ground area illuminated by the laser to a much greater extent than is ever

seen in ranging to an extended target array on a satellite. More importantly, the "target trajectory" (in this case the random height variability of the surface under investigation) is not a simple slope or even somewhat predictable as it is in the ranging or transponder case. Nevertheless, one can place constraints on the nominal maximum surface slope and roughness, which in turn place limits on the size of an individual range bin. Also, abrupt changes or discontinuities in range (e.g. a steep cliff) are now possible, and the autotracking algorithms must be clever enough to recognize these sudden transitions. This can be accomplished by applying both forward-looking and backward-looking predictor/corrector techniques to the data (see the next section). A third complication results from the fact that, unlike the ranger and transponder cases, there may be more than one valid trajectory resulting from reflections off multiple surfaces (e.g. cloud tops, planetary boundary layers, tree canopies, buildings, and ground surface returns). In the airborne instrument, we have dealt with this by porting the photomultiplier outputs into two receiver channels: (1) a coarse channel with 75 cm resolution which monitors single photon returns from virtually the entire path between the aircraft and ground; and (2) a fine channel with 5 cm resolution which concentrates on ground and near-ground (tree canopies, buildings, etc) returns. The ground return from the coarse receiver is used to set the gate center and width (typically a few microseconds) on the fine receiver.

Figure 5 shows a simulation of the airborne microaltimeter operated in a non-scanning mode during daylight. The unenhanced signal data from the simulated surface in the crude resolution O-C plot in Figure 5a shows up clearly against the solar background within the 4 μsec gate and reveals the presence of a simulated 50 meter cliff. Figure 5b, which has a much finer vertical and horizontal resolution, shows the points selected by the auto-tracking algorithm for a terrain segment to the right of the cliff and demonstrates the actual roughness of the simulated surface, which appears flat in the crude vertical scale of Figure 5a. Note that there are only a few obvious outlying points, which represent noise counts occurring randomly within the selected signal bins. These would be eliminated in iterative applications of the auto-tracking algorithm during post-flight data analysis.

Simulations of Earth and Mars orbital missions have demonstrated the ability of the microaltimeter approach to perform kHz rate surface measurements with telescope apertures on the order of 15 cm and single pulse energies on the order of 1 mJ or less [Degnan and McGarry, 1998; Degnan, 2000]. Because the temporal coherence of the return signal is much poorer for altimeters than for rangers or transponders, altimetry experiments normally require a higher mean signal return than rangers or transponders for effective discrimination against background noise. In designing the instrument, we typically target about 1 pe per detector pixel per laser fire for a nominal worst case slope and surface reflectance in order to achieve high probabilities of detection (75% to 100%) over most surfaces. Over bright surfaces such as snow and ice, the noise background can be so high that signal contrast can be lost when either the detector or ranging receiver has a dead-time longer than the temporal width of the surface return [Degnan, 2000]. Thus, our developmental microaltimeters use computer-controlled attenuators in the receiver to reduce the noise background and maintain signal cell contrast.

6. POST-DETECTION POISSON FILTERING AND CORRELATION RANGE RECEIVERS

A ***correlation range receiver*** (CRR) can be used to distinguish surface reflections from background noise counts during daylight operations [Degnan and McGarry, 1997]. In describing the operation of a CRR, we will consider the most complicated of the three systems - the photon counting altimeter. The CRR measures photon time-of-flight at multi-kilohertz rates relative to the outgoing pulse, and, in spaceborne or very high repetition rate airborne applications, must be able to handle multiple pulses in flight. With each laser fire, the CRR is gated to accept only those photons which enter the receiver during a time period in which surface returns are expected, and it can record multiple photon "stop" events which occur within the range gate. Software within the CRR breaks each ***range gate*** (along the vertical range axis) into a set of equal duration ***range bins*** as in Figure 7. A set of sequential laser fires along the horizontal (time) axis forms a ***frame***. The ***range bin width***, τ_b, in the CRR is chosen to accommodate all likely signal photon arrival times from a single surface occurring within a frame as defined by a ***frame sampling interval***, τ_f. The 2-D area defined by the horizontal range bin and vertical frame boundaries respectively in Figure 7 is called a ***cell***. A set of M contiguous frames forms a ***superframe***. Figure 7 shows a superframe consisting of 10 frames. The terrain is shown as a solid black line passing through the various cells. In the case of a ranger or

transponder with imperfect range-rate modeling, the range data would fall along a simple slope over the duration of the superframe.

Software in the CRR tentatively identifies the signal cell by summing the counts in each cell and comparing the total to a frame threshold value, K_{opt}, which is optimally chosen based on Poisson statistics. It is important that the frame threshold be high enough so that the number of noise cells falsely identified as signal is appropriately low but, at the same time, low enough so that one does not inadvertently dismiss the signal cell as noise. Because of the potentially large number of cells in a frame (especially during target acquisition when range uncertainties and gate widths are largest), a modest number of noise cells can be falsely identified as signal even when the probability of false alarm for any given cell is relatively small. It has been shown elsewhere [Degnan, 2000] that the optimum frame threshold is given by

$$K_{opt} = \frac{N_s + \ln(N_{bin})}{\ln\left(1 + \frac{N_s}{N_b}\right)} \tag{8}$$

where N_{bin} is the number of range bins within the gate (or equivalently cells within a frame) and N_s and N_b are the mean number of signal and noise counts respectively per cell. The choice of this threshold maximizes the ***differential cell count***, defined as the number of correctly identified signal cells minus the number of incorrectly identified noise cells (false alarms) in a superframe. During initial acquisition of the surface, N_s and N_b are based on a priori worst case expectations but can be replaced and/or updated in flight using actual counts once data is acquired.

If the count exceeds the threshold, the cell is tentatively identified as containing signal (the gray cells in Figure 7); otherwise, it is tentatively identified as containing noise (the white cells in Figure 7). Figure 7 also illustrates a situation where a steeper than average surface slope or highly modulated terrain causes the signal counts in a frame to fall into two or more cells with the result that none of the cells in frames 3, 7, and 8 achieve frame threshold. It is also statistically possible that a noise cell is occasionally mistakenly identified as signal. Under these weaker signal to noise conditions, further confirmation of signal acquisition can be obtained, if necessary, by applying an ***N of M test*** [Titterton et al., 1998] to the data which requires that, in N of M successive frames making up a superframe, a cell (1) passes the threshold test and (2) is displaced from signal cells in adjacent frames by no more than one range bin in the vertical (range) direction. We refer to this condition as a ***valid trajectory***. A sample of a valid trajectory for the altimeter, in which the signal cells exceed threshold in 7 of 10 frames, is illustrated in Figure 7.

More sophisticated tracking algorithms, which look forward and backward along the time axis, are possible and can further improve the accommodation of steep or rapidly modulated terrain features and recover missing data. For example, looking forward in time and using our adjacent range bin criteria, the lost signal in frame 3 is expected to occur in bin 4,5, or 6 (cells with upwardly sloped lines) since bin 5 was identified as the signal in Frame 2. However, looking backward in time from frame 4 suggests that bins 6,7, and 8 are the likely candidates in Frame 3 (cells with downwardly sloped lines). The only cell common to both the forward and backward groupings in Frame 3 is bin 6 (cross-hatched), which in reality contains most of the signal.

As a second example, we consider Frames 7 and 8 where the signal cell goes undetected in two consecutive frames. Looking forward in time from Frame 6 suggests the signal may be in bins 6 through 8 in frame 7 and bins 5 through 9 in Frame 8. Looking backwards in time from Frame 9 suggests bins 4 through 6 in Frame 8 and 3 through 7 in Frame 7. The overlapping (cross-hatched) bins are 6 and 7 in Frame 7 and bins 5 and 6 in Frame 8 which indeed contain the missing signal counts. While very abrupt changes in terrain (such as a steep cliff) can cause the signal cell to jump many range bins in a single frame and violate our $\pm$ one bin criteria, we saw in our earlier simulation (Figure 6) that the algorithm quickly identifies the surface at the new elevation.

7. SUMMARY

In summary, photon-counting, microlaser-based instruments:

- Require smaller power-aperture products than conventional high SNR systems. This implies a lighter, more compact instrument with reduced power consumption and lower fabrication costs. These qualities make it especially attractive for use in spaceborne missions, both Earth orbit or interplanetary.
- Offer orders-of-magnitude increase in sampling rates and spatial resolution. In rangers and transponders, the instrument rapidly drives down random errors and reproduces the target array/source impulse response for improved accuracy in the range data. In altimeters using detector arrays or segmented anode photomultipliers, one can approximate "point-to-point ranging" and "quasi-3D imaging" by measuring the round-trip flight times of individual photons to achieve improved resolution in both the transverse and vertical coordinates. In addition, the smaller system apertures and kilohertz repetition rates greatly expand the options for scanning the beam to achieve improved along-track and/or cross-track visualization and resolution.
- Result in lower single pulse radiation fluxes both on the ground and within the instrument. This increases system reliability by reducing the risk of internal optical damage and improves the margin of safety for ground-based observers.
- Further improves system reliability and ranging accuracy through the use of small, monolithic, passively Q-switched, microlaser transmitters which are extremely simple in their construction and operation, require no failure-prone high speed or pulsing electronics, and never go out of alignment.

For simplicity, we have limited our discussion in this paper to the observation of "hard" targets (a satellite reflector, bare terrain, or a distant laser) against a solar background, but we believe the techniques discussed here can be applied to any kHz airborne or spaceborne lidar where the expected mean signal response is at the 0.1 pe level or higher and viewed as quasi-temporally coherent, i.e. the signal counts can be collected within microsecond scale gates in O-C space over time frames of a few milliseconds. Examples include the detection of "distributed" or "soft" targets such as buildings , tree canopies and sub-canopies [Priedhorsky et al, 1996] as well as laser-induced flourescence experiments used to monitor crop health, ocean health via photoplankton populations, etc.

REFERENCES

Abbott, R., Shelus, P., 1973, Laser observations of the Moon: Identification and construction of normal points for 1969-1971, The Astronomical Journal 78, pp. 784-793.

Degnan, J., 1993, "Millimeter Accuracy Satellite Laser Ranging: A Review", in Contributions of Space Geodesy to Geodynamics: Technology, D. E. Smith and D. L. Turcotte (Eds.), AGU Geodynamics Series, Volume 25, pp. 133-162.

Degnan, J., 1996, "Compact laser transponders for interplanetary ranging and time transfer", Proc. 10th International Workshop on Laser Ranging, pp. 24-31, Shanghai, China, November 11-15.

Degnan, J., McGarry, J., 1997, "SLR2000: Eyesafe and autonomous satellite laser ranging at kilohertz rates", SPIE Vol 3218, Laser Radar Ranging and Atmospheric Lidar Techniques, pp. 63-77, London, UK, Sept. 24-26.

Degnan, J., 1998, "SLR2000 Project: Engineering Overview and Status", Proc. 11th International Workshop on Laser Ranging, pp. 389-398, Deggendorf, Germany, Sept. 21-25.

Degnan, J., McGarry, J., Dabney, P., Zagwodzki, T., Tierney, M., Weatherley, M., 1998, "Design and Test of a Breadboard Interplanetary Laser Transponder", Proc. 11th International Workshop on laser Ranging, pp. 716-728, Deggendorf, Germany, Sept. 21-25.

Degnan, J., McGarry, J., 1998, "Feasibility study of Multikilohertz Spaceborne Microlaser Altimeters", European Geophysical Society (EGS) Symposium, Nice, France, April 20-24. Annales Geophysicae, Part

1, Society Symposia, Solid Earth Geophysics and Geodesy, Supplement 1 to Volume 16, p. C379 (Abstract only).

Degnan, J., 2000, " Photon-counting Multikilohertz Microlaser Altimeters for Airborne and Spaceborne Topographic Measurements", submitted to J. Geodynamics.

Priedhorsky, W., Smith, R., Ho, C., 1996, "Laser ranging and mapping with a photon counting detector", Applied Optics 35, pp.441-452.

Titterton, P., Sweeney, H., Leonard, D., 198, "System/Usage Impact of Operating the SLR2000 at 2 kHz", Proc. 11th International Workshop on Laser Ranging, Deggendorf , Germany , pp. 426-437, September 21-25.

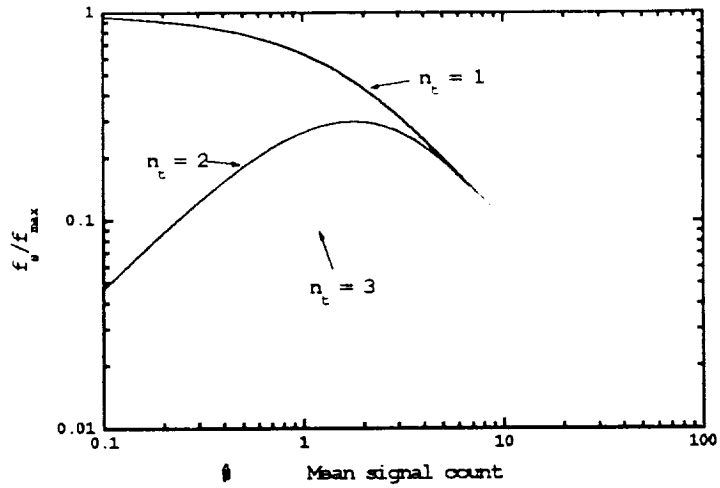

Figure 1. Normalized signal return rate as a function of mean signal strength and receiver detection threshold.

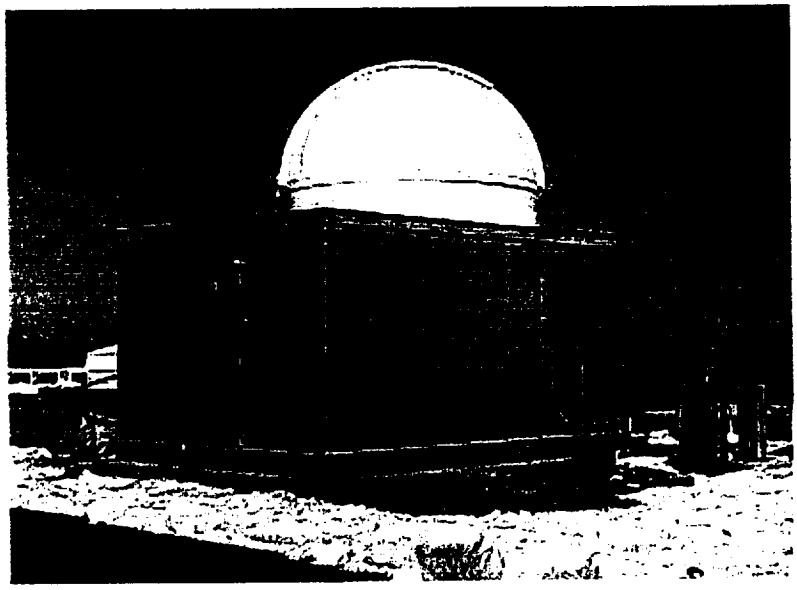

Figure 2. Prototype SLR2000 Ranging System at the Goddard Space Flight Center.

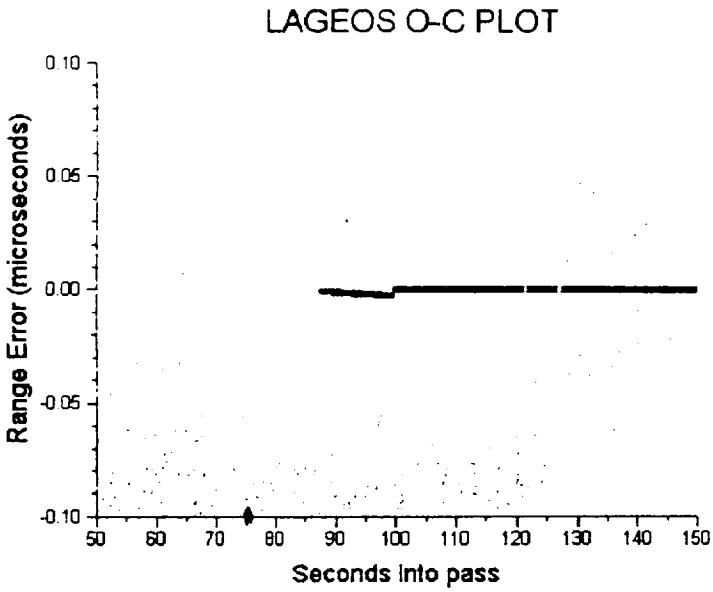

Figure 3. Simulated SLR2000 acquisition of the LAGEOS satellite at 20 degrees elevation (8300 km).

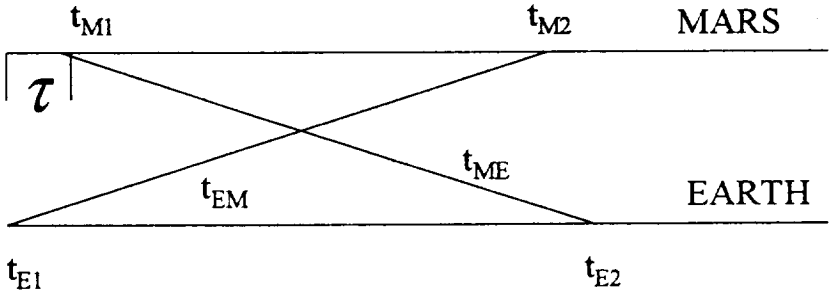

Figure 4: Timing diagram for an Asynchronous Laser Transponder Link

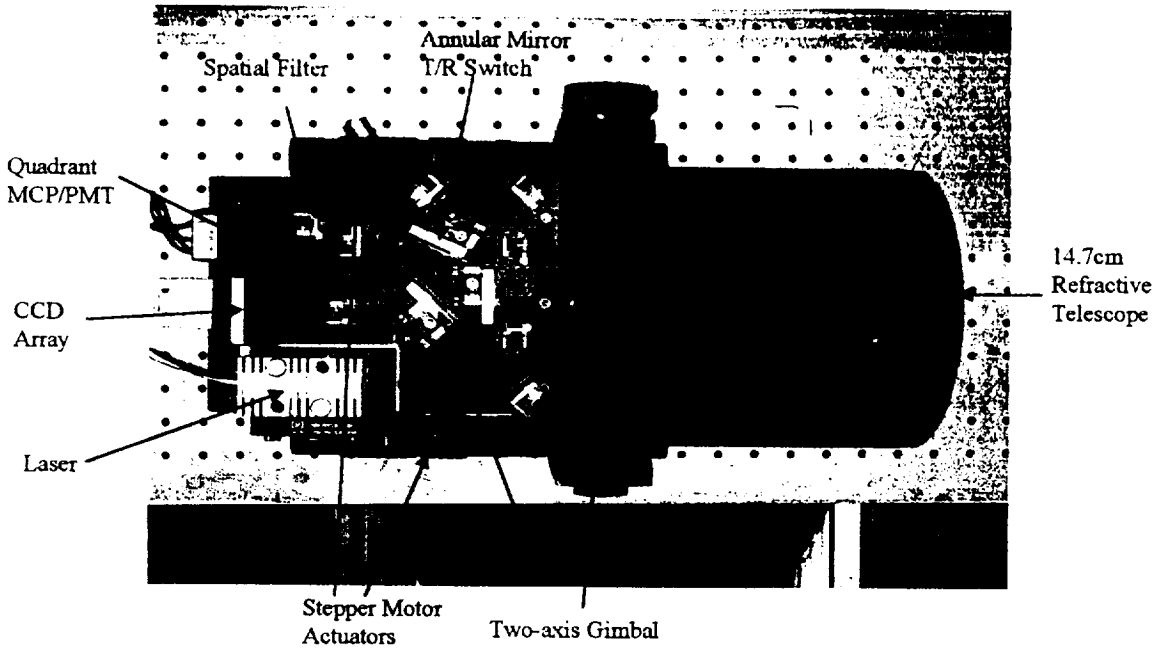

Figure 5: Top view of NASA's Breadboard Interplanetary Laser Transponder which is sized for an Earth-Mars link with SLR2000.

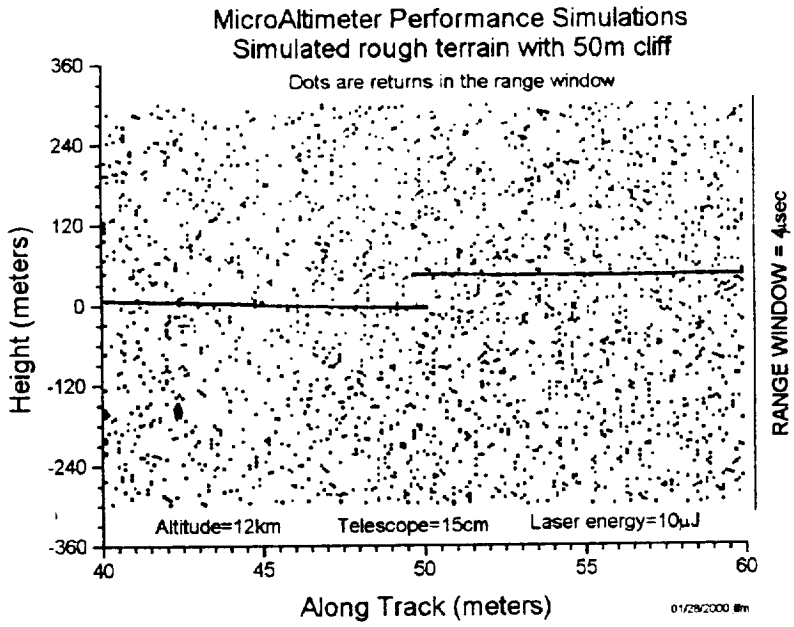

(a)

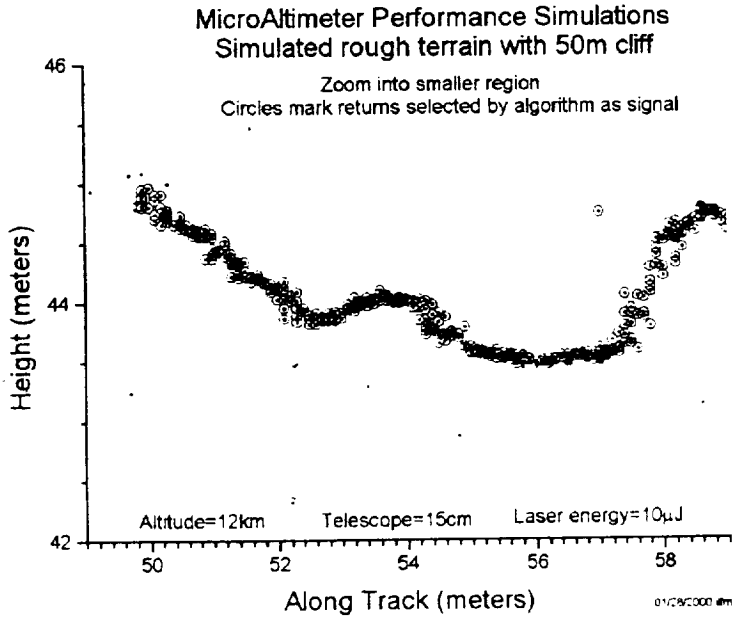

(b)

Figure 6: Simulation of NASA's Airborne Multikilohertz Microlaser Altimeter ("Microaltimeter") operating from a cruise altitude of 12 km.

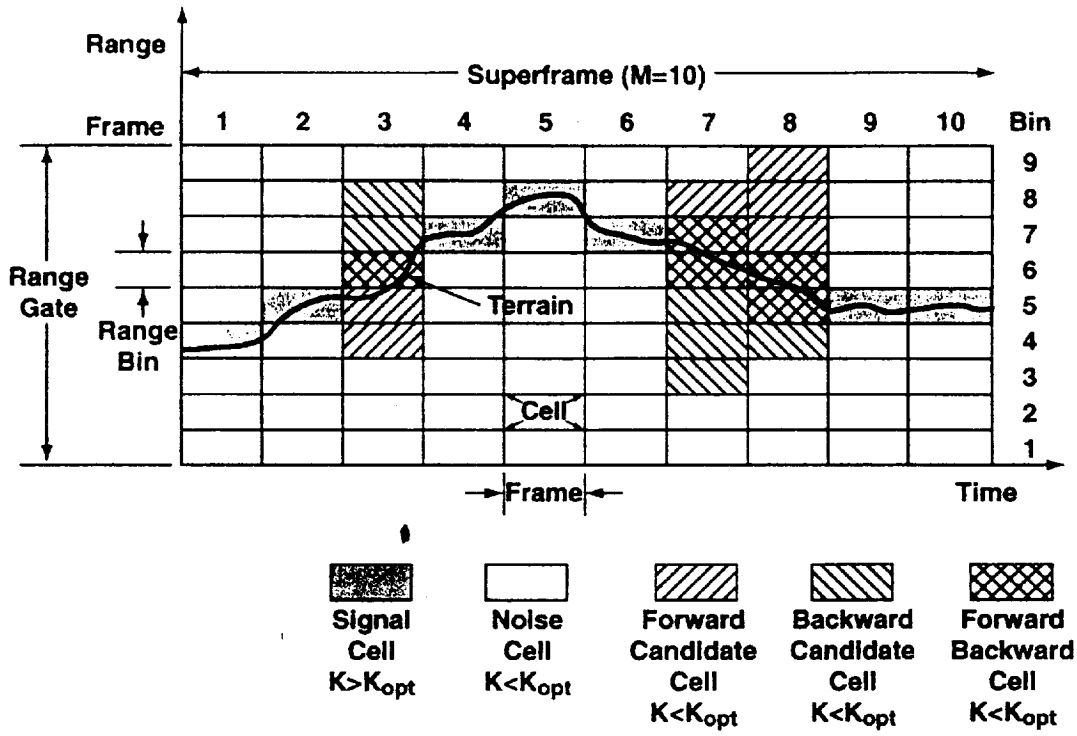

Figure 7: Correlation Range Receiver basics as applied to a photon counting altimeter.